Chaos, Solitons and Fractals 188 (2024) 115475

Contents lists available at ScienceDirect

Chaos, Solitons and Fractals

journal homepage: www.elsevier.com/locate/chaos

A general deterministic model of ordinary differential equations for a broad variety of different diseases

Christoph Sticha [a,b], Francesco Picasso [b,a], Christina Kuttler [c], Michael Hoelscher [b,a,d,e], Andreas Wieser [a,b,d,f], Noemi Castelletti [b,a,g,*]

[a] Fraunhofer Institute for Translational Medicine and Pharmacology ITMP, Immunology, Infection and Pandemic Research, Munich, Germany
[b] Institute of Infectious Diseases and Tropical Medicine, LMU University Hospital, LMU Munich, Munich, Germany
[c] Department of Mathematics, Technical University of Munich, Garching, Germany
[d] German Centre for Infection Research, Partner Site Munich, Munich, Germany
[e] Unit Global Health, Helmholtz Zentrum München, German Research Center for Environmental Health (HMGU), Neuherberg, Germany
[f] Max von Pettenkofer Institute for Hygiene and Medical Microbiology, LMU Munich, Munich, Germany
[g] Institute of Radiation Medicine, Helmholtz Zentrum München, Neuherberg, Germany

ARTICLE INFO

Keywords:
General epidemic model
Ordinary differential equations
Reproduction rate
Compartmental model
Epidemic control
Numerical simulation

ABSTRACT

The COVID-19 pandemic underscored the pivotal role of mathematical models in comprehending pandemic dynamics and making accurate predictions under diverse interventions. Various mathematical models, particularly deterministic ones, have proven valuable for analyzing the impact of political, social, and medical measures during ongoing pandemics. In this study, we aim to formulate and characterize a comprehensive model applicable to different infectious diseases. Reviewing numerous disease-specific models reveals a common foundation in the Kermack–McKendrick model (SIR model). While there are more general versions incorporating population dynamics, vector populations, and vaccination, none encompass all attributes simultaneously. To address this gap, we propose a comprehensive general model capable of accommodating different transmission modes, pandemic control measures, and diverse pathogens. Unlike disease-specific models, having such a pre-established model with foundational mathematical properties analyzed eliminates the need to reevaluate these characteristics for each new disease-specific model. This article presents our comprehensive general model, supported by mathematical analysis and numerical simulations, offering a versatile tool for understanding the dynamics of emerging infectious diseases and guiding intervention strategies. The applicability of the model is demonstrated through simulations.

1. Introduction

The COVID-19 pandemic highlighted the crucial role of mathematical models in comprehending the fundamental dynamics of a pandemic and making accurate predictions regarding its future course under various interventions [1–5]. Similar to previous infectious diseases, like influenza, HIV or measles, a diverse range of mathematical models have been developed specifically for the COVID pandemic [6–8]. In particular, deterministic models have been helpful for analyzing the impact of political, social and medical measures in an ongoing pandemic. In this study, our objective is to formulate and characterize a comprehensive model applicable to various types of infectious diseases. Consequently, we have undertaken a thorough review of numerous models pertaining to different diseases as described in the following. All of them rely on the basic principles of the Kermack–McKendrick model (sometimes also referred to as SIR model), including three compartments for susceptible (S), infected (I), and recovered (R) individuals together with their transition rates, where recovered individuals are assumed to be immune [9]. There are already some more general and extended versions of this model, including for example population dynamics like birth and death processes or additional transitions directly turning susceptible into recovered individuals to incorporate vaccination [10]. Sometimes vector-borne diseases are described by additional compartments for a vector population [11]. Others include vaccination (V) via an additional compartment ($SVIR$ model) [12] or a latent phase via an additional exposed (E) compartment ($SEIR$ model) and including a transition back from R to S as immunity vanishes over time for some diseases [13]. Arias and colleagues [7] developed a model for the spread of HIV, adding a second stage of infection to the

* Corresponding author at: Institute of Infectious Diseases and Tropical Medicine, LMU University Hospital, LMU Munich, Munich, Germany.
E-mail address: Noemi.Castellitti@med.uni-muenchen.de (N. Castelletti).

https://doi.org/10.1016/j.chaos.2024.115475
Received 28 May 2024; Received in revised form 7 August 2024; Accepted 30 August 2024
Available online 7 September 2024

SIR model for those individuals, where the HIV infection already resulted in manifest AIDS stadium. There are several models for the spread of measles. Memon et al. [8] combined the $SEIR$ and the $SVIR$ model including both, an exposed state and a vaccination compartment to an $SVEIR$ model. Another work by Alemneh and Belay [14] suggested to leave out the exposed compartment but include a pathogen (P) that can be spread in the environment, focusing on smear infections. A similar approach is chosen to include reservoirs of hepatitis A viruses in food or water by Mwaijande and Mpogolo [15]. In 2019, Aldila and Asrianti [16] suggested to enrich a SVIR model by a second vaccination compartment (V_2) and an additional compartment for quarantined individuals (Q). Verguet and colleagues [17] decided to separate the vaccination into three compartments for vaccinated susceptibles, infecteds and recovereds, allowing also for vaccination of infected and recovered individuals in their modification of a $SVIR$ model for measles. For tick borne encephalitis, Akram et al. [18] developed a SEI model without a recovered compartment but including a vector population consisting of susceptible and infected ticks. For Malaria there are also vector populations considered together with either the possibility to relapse into infection from the recovered compartment or with waning immunity turning recovered individuals into susceptible ones over time [19,20]. Kanyiri et al. [6] suggested an Influenza model with a distinction between a wild-type and a resistant infection (I_w and I_r). Some models for avian influenza completely leave out the vector population and model the spread with a $SVEIR$ model, as the main spread occurs in inter human contacts [21]. Other models distinguish the vector population in separate compartments for a wild bird population and a population of domestic birds [22,23].

To assess specific research questions, especially during the COVID pandemic, very extended models have been developed. Considering hospitalization rates as a possible indicator for the course of the COVID pandemic, Fuderer and colleagues [3] developed a model not only including vaccinations, but also compartments for detected and undetected infections and further diversifying in the different courses of the disease like individuals under intensive care treatment. A similar approach has been used in a cooperation with Contento and colleagues [2] for an integrative modeling of different characteristic measures.

However, to the best of our knowledge, there is currently no comprehensive model available that encompasses all the attributes described above simultaneously, and is not limited to a specific pathogen. Nevertheless, in cases of new pathogens carrying the potential threat of evolving into an epidemic, having a pre-existing detailed model on hand could prove useful. Such a model should be able to cope different ways of transmission, including direct human interaction, as well as pathogen spreading through smear infections or vector populations. Additionally, it should consider pandemic control measures like vaccination campaigns and quarantine protocols. Having such a model pre-established, with foundational mathematical properties already analyzed, eliminates the need to reevaluate these characteristics for every new deterministic model tailored to a specific disease. This article proposes a comprehensive general model, supported by mathematical analysis and numerical simulations for illustrative purposes.

2. Materials and methods

Our approach to define a comprehensive general model capable of describing the spread of various infectious diseases is based on a deterministic system of ordinary differential equations (ODEs). The model structure is initially idealized as a general SIR model by Kermack and McKendrick [9], which is then expanded by incorporating several compartments identified in the literature as relevant for different diseases.

An illustration of the final model is provided in Fig. 1.

An additional exposed state (E) was introduced to the standard SIR model, representing individuals exposed to the disease, infected but asymptomatic, not yet infectious, and not detectable [12]. Drawing inspiration from HIV models, a second stage of infection (I_2) was included to capture diseases that progress through different stages [7,24]. These two stages could for example be a pre-symptomatic and a symptomatic phase. To accommodate vaccination modeling, two vaccination compartments (V_1 and V_2) were added to represent the effect of up to two doses of vaccination. As most of the reviewed models only incorporated no or a maximum of two doses of vaccination, this should be sufficient for this general purpose in the onset of a new epidemic. At a time when more than two doses of a vaccine are implemented, probably more detailed models are used for specific investigations anyways, what is out of scope for this general work. Previous models for measles [14,16], avian influenza [21] and influenza [6] already underlined the importance of these compartments. The COVID-19 pandemic further emphasized the need to consider both detected and undetected infected individuals, leading to the introduction of detected compartments (D_1 and D_2) for each infection stage. Since a person can either be detected or undetected, the stages can be considered mutually exclusive, with I_1 and I_2 functioning as the corresponding non-detected infected compartments. The inclusion of undetected compartments facilitates the parameterization of testing strategies, laboratory capacities and quarantine measures.

To ensure comprehensiveness, the model not only considers direct inter-human transmissions but also incorporates infections from external pathogens. For transmissions via pathogens spread by infected humans in the environment, an additional compartment P is added, akin models for measles or Ebola [14,25]. For other diseases primarily transmitted by vectors, a population of susceptible (S_V) and infected (I_V) vector individuals, along with corresponding population dynamics, is included. This modeling approach has proven successful for diseases such as avian influenza, malaria and tick-borne encephalitis [18–20,22,23,26]. As the aim of this model is to study human epidemic dynamics in an early stage of infection, more detailed vector dynamics are left out here, as they would afford more detailed knowledge and data about vector dynamics.

The general model not only consists of compartments but also includes several possible transitions illustrated as arrows in Fig. 1 and extensively described in Table 1. In case a stage of the model is unnecessary for disease representation, it can be easily adapted by "switching off" compartments, setting all in- and outgoing transition rates to zero. This adaptability allows for modeling diseases without latency or with only one distinguishable stage of infection. For example, direct transition paths connecting S to I_1 (skipping E) can be generated by setting $a_1 = a_2 = 0$, and a direct transition from I_1 to R (skipping I_2) via $a_3 = a_4 = 0$. Similarly, if there is no second stage of infection and, therefore, no second stage for detected individuals D_2, a transition from D_1 to R is easily possible. Modeling the event of a vaccinated individual getting infected can be done either with a direct transition to the exposed state E if included in the model, or directly to I_1. A transition from R back to S accounts for possible waning immunity after recovery, while a regression to the infectious state involves transitioning from R back to I_1. The latter event has proven to be significant in modeling diseases like malaria involving a hypnozoite, a dormant form of the parasite that may persist in the liver, leading to reactivation [19,27]. This general and flexible model can be easily customized to accommodate various scenarios.

The general population dynamics are introduced to the model through a constant birth term Δ and a *per capita* death rate μ (see Eq. (1)). For the sake of simplicity this model assumes every newborn to be susceptible, neglecting infection during birth or maternal immunity. The vector population dynamics are similarly included through corresponding parameters Δ_V and μ_V in Eqs. (10) and (11). The environmental pathogen arises at rate α_P Eq. (12), depending on the infective human population, and vanishes at rate μ_P. The death rate for infected individuals might differ from

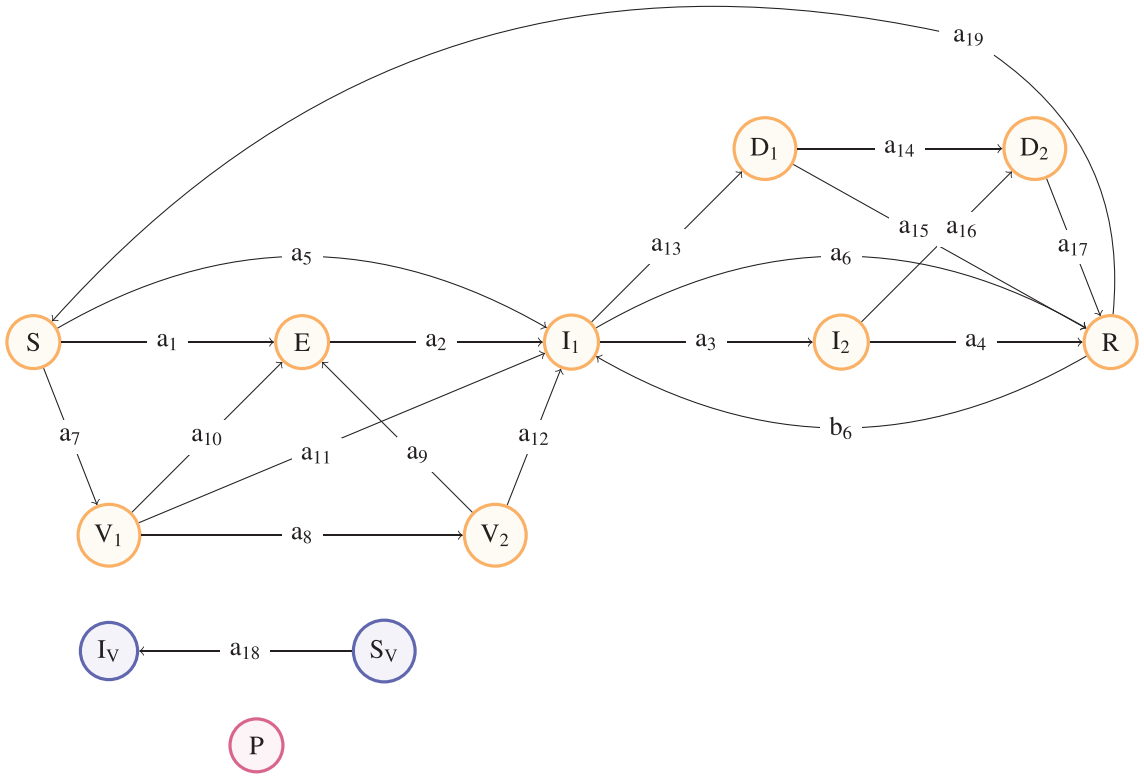

Fig. 1. Overview of the general model. The mutually exclusive compartments are illustrated as human (orange), vector (blue) or external pathogen (red) nodes. The compartments are susceptibles (S), exposeds (E), stage one infecteds (I_1), stage two infecteds (I_2), stage one detected infecteds (D_1), stage two detected infecteds (D_2), recovereds (R), first dose vaccinateds (V_1), second dose vaccinateds (V_2), susceptible vectors (S_V), infected vectors (I_V) and an environmentally spread pathogen (P). The possible transition paths are depicted as arrows. Birth and death processes are left out here for clarity even though they are considered in the system of ODEs.

the death rate of non-infected individuals and is given as μ_{I_1} and μ_{I_2} for both stages of infection in Eqs. (3), (4), (8) and (9). The infection occurs at rate λ (human population) or λ_V (vector population). The different transition rates are numbered from a_1 to a_{19} and b_6 (for the backward transition opposing a_6). The infectiousness of a person is denoted by f_{I_1}, f_{I_2} and f_D, being potentially different for the stages of infection. Notably, the parameter f_D enables the quantification of behavioral changes or quarantine measures for detected individuals, with $f_D \leq 1$ signifying a reduction in their contribution to infections. Consequently, there is no necessity to introduce an additional quarantine compartment, as seen in some other articles [28].

$$\frac{dS}{dt} = \Delta + a_{19}R - a_1\lambda S - a_5\lambda S - a_7 S - \mu S \quad \text{Susceptible} \quad (1)$$

$$\frac{dE}{dt} = a_1\lambda S + a_{10}\lambda V_1 + a_9\lambda V_2 - a_2 E - \mu E \quad \text{Exposed} \quad (2)$$

$$\frac{dI_1}{dt} = a_2 E + a_5\lambda S + a_{11}\lambda V_1 + a_{12}\lambda V_2 - \left(a_3 + a_6 + a_{13}\right) I_1 + b_6 R - \mu_{I_1} I_1 \quad \text{Infected (1st stage)} \quad (3)$$

$$\frac{dI_2}{dt} = a_3 I_1 - \left(a_4 + a_{16}\right) I_2 - \mu_{I_2} I_2 \quad \text{Infected (2nd stage)} \quad (4)$$

$$\frac{dR}{dt} = a_4 I_2 + a_6 I_1 + a_{15} D_1 + a_{17} D_2 - b_6 R - a_{19} R - \mu R \quad \text{Recovered} \quad (5)$$

$$\frac{dV_1}{dt} = a_7 S - a_8 V_1 - \left(a_{10} + a_{11}\right)\lambda V_1 - \mu V_1 \quad \text{Vaccinated (1st dose)} \quad (6)$$

$$\frac{dV_2}{dt} = a_8 V_1 - \left(a_9 + a_{12}\right)\lambda V_2 - \mu V_2 \quad \text{Vaccinated (2nd dose)} \quad (7)$$

$$\frac{dD_1}{dt} = a_{13} I_1 - \left(a_{14} + a_{15}\right) D_1 - \mu_{I_1} D_1 \quad \text{Detected (1st stage)} \quad (8)$$

$$\frac{dD_2}{dt} = a_{14} D_1 + a_{16} I_2 - a_{17} D_2 - \mu_{I_2} D_2 \quad \text{Detected (2nd stage)} \quad (9)$$

$$\frac{dS_V}{dt} = \Delta_V - a_{18}\lambda_V S_V - \mu_V S_V \quad \text{Susceptible vector} \quad (10)$$

$$\frac{dI_V}{dt} = a_{18}\lambda_V S_V - \mu_V I_V \quad \text{Infected vector} \quad (11)$$

$$\frac{dP}{dt} = \alpha_P \cdot \left(f_{I_1} I_1 + f_{I_2} I_2 + f_D\left(f_{I_1} D_1 + f_{I_2} D_2\right)\right) - \mu_P P \quad \text{Environmental pathogen} \quad (12)$$

Table 1
Parameter overview.

Parameter	Description
$\hat{a}_1, \hat{a}_5, a_1, \ldots, a_{19}$	transition rates between compartments
b_6	backwards transition from R to I_1 (opposing a_6) for relapse/reactivation
f_{I_1}, f_{I_2}, f_P	fractions (or multiples) of base infectiousness for 1st stage infected, 2nd stage infected humans or environmental pathogen
f_D	≤ 1 fraction of infectiousness for detected individuals as they might be quarantined or due to behavioral changes
e_1, e_2	efficacy of 1st and 2nd dose of vaccine
Δ (and Δ_V)	birth term for human (and vector) population
α_P	onset rate for environmental spread of pathogen
μ (and μ_V, μ_P)	death rate of humans (and vectors/pathogen)
μ_I	additional death rate for infected humans in cause of the disease
$f_{\mu_{I_2}}$	fraction or multiple deadliness for 2nd stage of infection
δ_{HH}, δ_{VH}, δ_{HV}, δ_{VV}, δ_{PH}	$\in \{0,1\}$ indicators whether transmissions are taking place (= 1) or not (= 0) from H(uman)→H, V(ector)→H, H→V, V→V, P(athogen)→H

For analysis purposes, the ODE system was re-parameterized, defining either combinations of fixed parameters or functions depending on the compartment variables and/or time.

$$N = S + E + I_1 + I_2 + R + V_1 + V_2 + D_1 + D_2 \quad \text{Total human population} \tag{13}$$

$$N_V = S_V + I_V \quad \text{Total vector population} \tag{14}$$

$$\phi_H = \begin{cases} 0 & \text{for } N = 0 \\ \frac{f_{I_1} I_1 + f_{I_2} I_2 + f_D\left(f_{I_1} D_1 + f_{I_2} D_2\right)}{N} & \text{else} \end{cases} \quad \text{Total infective humans (weighted)} \tag{15}$$

$$\phi_V = \begin{cases} 0 & \text{for } N_V = 0 \\ \frac{I_V}{N_V} & \text{else} \end{cases} \quad \text{Total infective vectors} \tag{16}$$

$$\phi_P = \begin{cases} 0 & \text{for } N = 0 \\ \frac{f_P P}{N} & \text{else} \end{cases} \quad \text{Infective pathogen} \tag{17}$$

$$\lambda = \delta_{HH} \cdot \phi_H + \delta_{VH} \cdot \phi_V + \delta_{PH} \cdot \phi_P \quad \text{Transmission rate (humans)} \tag{18}$$

$$\lambda_V = \delta_{HV} \cdot \phi_H + \delta_{VV} \cdot \phi_V \quad \text{Transmission rate (vector)} \tag{19}$$

$$\mu_{I_1} = \mu_I + \mu \quad \text{Death rate (1st stage infection)} \tag{20}$$

$$\mu_{I_2} = f_{\mu_{I_2}} \cdot \mu_I + \mu \quad \text{Death rate (2nd stage infection)} \tag{21}$$

$$a_1 = f_1 \cdot \hat{a}_1 \tag{22}$$

$$a_5 = f_1 \cdot \hat{a}_5 \tag{23}$$

$$a_9 = \left(1 - e_2\right) \cdot a_1 \tag{24}$$

$$a_{10} = \left(1 - e_1\right) \cdot a_1 \tag{25}$$

$$a_{11} = \left(1 - e_1\right) \cdot a_5 \tag{26}$$

$$a_{12} = \left(1 - e_2\right) \cdot a_5 \tag{27}$$

$$f_1(t) = \text{ some fluctuant function} \quad \text{varying force of infection (e.g. seasonality)} \tag{28}$$

The total population N is the sum of all human compartments, as defined in Eqs. (13). Similarly the vector population N_V is computed as described in Eq. (14). The global infective term ϕ_H is defined as the weighted mean of the various infectiousness rates, with the total population N serving as denominator. This formulation enables biologically interpretable parameter values, as expressed in Eq. (15). Analogously, ϕ_V Eq. (16) and ϕ_P Eq. (17) are defined for infection via vectors or an environmental pathogen, with f_P scaling the infectiousness per pathogen unit. The infectiousness is incorporated into the transmission rates λ and λ_V (for vector population infection), consisting of ϕ_H, ϕ_V and ϕ_P along with corresponding indicator functions $\delta \in \{0,1\}$ indicating the relevant transmission routes for a specific pathogen. For instance, $\delta_{VH} = 1$ signifies the potential transmission from an infected vector to a susceptible human; otherwise, $\delta_{VH} = 0$. As a disease might elevate the death rate of infected individuals, the corresponding death rates are defined as the sum of the base death rate μ and the additional mortality rate of the disease μ_I Eq. (20). Considering potential variations in mortality during the second stage of infection, a factor $f_{\mu_{I_2}}$ is introduced in the definition of μ_{I_2} Eq. (21). The efficacy of the first and second dose of vaccination is incorporated through e_1 and e_2 in Eqs. (24)–(27). To account for potential variations in the course of infection due to seasonality or pandemic measures, a time-dependent fluctuation function f_1 Eq. (28) influences a_1 and a_5 Eqs. (22) and (23).

All parameters, including $f_1(t)$ (for $t \geq 0$), are assumed to be non-negative and are comprehensively summarized in Table 1.

3. Results

In order to proof basic analytical properties and general applicability of the model, it is analyzed in the following analytically and numerically.

3.1. Analytical results

First the model is investigated for existence, uniqueness and non-negativity of solutions as well as for boundedness, a disease-free equilibrium and the basic reproduction rate.

3.1.1. Non-negativity and existence of a unique non-negative solution

Suppose, f_1 is a Lipschitz continuous function on $\mathbb{R}_{\geq 0}$. Then for $N > 0$ and $N_V > 0$, the whole system of ODEs is Lipschitz continuous. As the constant birth terms Δ and Δ_V assure S and S_V to be strictly positive, also N and N_V stay strictly positive.

Let $X := (S, E, I_1, I_2, R, V_1, V_2, D_1, D_2, S_V, I_V, P)$ and $X'(t) = f(t, X)$. Then the whole system stays non-negative for non-negative initial values if:

$$f_j(t, X)\Big|_{X_j=0} \geq 0 \text{ for } x \in \mathbb{R}^{12}_{\geq 0} \text{ and } t \geq 0$$

for all $j \in \{1, 2, \dots, 12\}$. So for $X \in \mathbb{R}^{12}_{\geq 0}$ with $N, N_V > 0$ we find:

$$S'|_{S=0} = \Delta + a_{19}R > 0 \tag{29}$$

$$E'|_{E=0} = a_1\lambda S + a_{10}\lambda V_1 + a_9\lambda V_2 \geq 0 \tag{30}$$

$$I_1'\Big|_{I_1=0} = a_2 E + a_5\lambda S + a_{11}\lambda V_1 + a_{12}\lambda V_2 + b_6 R \geq 0 \tag{31}$$

$$I_2'\Big|_{I_2=0} = a_3 I_1 \geq 0 \tag{32}$$

$$R'|_{R=0} = a_4 I_2 + a_6 I_1 + a_{15} D_1 + a_{17} D_2 \geq 0 \tag{33}$$

$$V_1'\Big|_{V_1=0} = a_7 S \geq 0 \tag{34}$$

$$V_2'\Big|_{V_2=0} = a_8 V_1 \geq 0 \tag{35}$$

$$D_1'\Big|_{D_1=0} = a_{13} I_1 \geq 0 \tag{36}$$

$$D_2'\Big|_{D_2=0} = a_{14} D_1 + a_{16} I_2 \geq 0 \tag{37}$$

$$S_V'\Big|_{S_V=0} = \Delta_V > 0 \tag{38}$$

$$I_V'\Big|_{I_V=0} = a_{18}\lambda_V S_V \geq 0 \tag{39}$$

$$P'|_{P=0} = \alpha_P \cdot \left(f_{I_1} I_1 + f_{I_2} I_2 + f_D\left(f_{I_1} D_1 + f_{I_2} D_2\right)\right) \geq 0. \tag{40}$$

This is sufficient to proof the existence of unique, non-negative solutions for all non-negative initial values to this system of ODEs with $S(0) > 0$ and $S_V(0) > 0$ [29].

3.1.2. Boundedness

Let $\mu > 0$, $\mu_V > 0$ and $\mu_P > 0$. By definition of the total population N one finds

$$N' = \Delta - \mu N - \mu_I(I_1 + D_1 + f_{\mu_{I_2}} I_2 + f_{\mu_{I_2}} D_2) \leq \Delta - \mu N \underset{\text{for } N > \frac{\Delta}{\mu}}{<} 0. \tag{41}$$

Therefore, the total population has an upper bound not to exceed a total population of $\overline{N} = \frac{\Delta}{\mu}$. As the compartments are all proven to be non-negative, all consistent compartments for the human population are bound, too. Similarly one finds $\overline{N_V} = \frac{\Delta_V}{\mu_V}$ as upper bound for the vector population and its compartments S_V and I_V. With that, one finds $\overline{P} = \frac{\alpha_P \cdot max\left\{f_{I_1}, f_{I_2}\right\}}{\mu_P} \cdot \overline{N}$ as an upper bound for P:

$$P' = \alpha_P \cdot \left(f_{I_1} I_1 + f_{I_2} I_2 + f_D\left(f_{I_1} D_1 + f_{I_2} D_2\right)\right) - \mu_P P \leq \alpha_P \cdot max\left\{f_{I_1}, f_{I_2}\right\} \cdot \overline{N} - \mu_P \overline{P} \leq 0 \tag{42}$$

Therefore, the whole system is upper-bounded.

3.1.3. Disease-free equilibrium

To find a disease-free equilibrium, $E = I_1 = I_2 = R = V_1 = V_2 = D_1 = D_2 = I_V = P = 0$ is assumed. This leads to $\lambda = \lambda_V = 0$ and hence:

$$S' = \Delta - a_7 S - \mu S \tag{43}$$

$$V_1' = a_7 S - a_8 V_1 - \mu V_1 \tag{44}$$

$$V_2' = a_8 V_1 - \mu V_2 \tag{45}$$

$$S_V' = \Delta_V - \mu_V S_V \tag{46}$$

$$E' = I_1' = I_2' = R' = D_1' = D_2' = I_V' = P' = 0 \tag{47}$$

which, as $\mu > 0$ and $\mu_V > 0$, solves for the unique disease-free equilibrium:

$$S^* = \frac{\Delta}{a_7 + \mu} \tag{48}$$

$$V_1^* = \frac{a_7 \Delta}{(a_7 + \mu)(a_8 + \mu)} \tag{49}$$

$$V_2^* = \frac{a_7 a_8 \Delta}{\mu (a_7 + \mu)(a_8 + \mu)} \tag{50}$$

$$S_V^* = \frac{\Delta_V}{\mu_V} \tag{51}$$

with $N^* = S^* + V_1^* + V_2^* = \frac{\Delta}{\mu}$ and $N_V^* = S_V^* = \frac{\Delta_V}{\mu_V}$. This equilibrium only exists (with positive populations N and N_V) as long as population dynamics are involved ($\Delta, \Delta_V, \mu, \mu_V > 0$).

3.1.4. Reproduction rate

As one of the most important and informative characteristic values of an epidemic model, the reproduction rate $\mathcal{R}_0$ cannot be missing. The method used in this analysis is the next generation matrix approach originally proposed by Diekmann and Heesterbeek in 1990 [30]. Following the van den Driessche and Watmough method as described by Maia Martcheva [11], the system is split into infected compartments $X = (E, I_1, I_2, D_1, D_2, I_V, P)$ and non-infected compartments $Y = (S, R, V_1, V_2, S_V)$. Next the right-hand side terms of X are split into new infections $\mathcal{F}$ and remaining dynamics $\mathcal{V}$:

$$\begin{aligned} X' =& \mathcal{F}(X,Y) - \mathcal{V}(X,Y) \\ =& \begin{pmatrix} a_1 \lambda S + a_{10} \lambda V_1 + a_9 \lambda V_2 \\ a_5 \lambda S + a_{11} \lambda V_1 + a_{12} \lambda V_2 + b_6 R \\ 0 \\ 0 \\ 0 \\ a_{18} \lambda_V S_V \\ \alpha_P \cdot \left(f_{I_1} I_1 + f_{I_2} I_2 + f_D \left(f_{I_1} D_1 + f_{I_2} D_2 \right) \right) \end{pmatrix} - \begin{pmatrix} a_2 E + \mu E \\ -a_2 E + \left(a_3 + a_6 + a_{13} \right) I_1 + \mu_{I_1} I_1 \\ -a_3 I_1 + \left(a_4 + a_{16} \right) I_2 + \mu_{I_2} I_2 \\ -a_{13} I_1 + \left(a_{14} + a_{15} \right) D_1 + \mu_{I_1} D_1 \\ -a_{14} D_1 - a_{16} I_2 + a_{17} D_2 + \mu_{I_2} D_2 \\ \mu_V I_V \\ \mu_P P \end{pmatrix}. \end{aligned} \tag{52}$$

This decomposition has to satisfy the following basic properties:

1. $\mathcal{F}_i(0, Y) = 0$ and $\mathcal{V}_i(0, Y) = 0$ for $Y \geq 0$ and $i = 1, \ldots, 7$
2. $\mathcal{F}_i(X, Y) \geq 0$ for all $X, Y \geq 0$
3. $\mathcal{V}_i(X, Y) \leq 0$ when $X_i = 0$ for $i = 1, \ldots, 7$
4. $\sum_{i=1}^{7} \mathcal{V}_i(X, Y) \geq 0$ for all $X, Y \geq 0$

This properties are clearly satisfied in our case (note that again $X = 0$ implies $\lambda = \lambda_V = 0$). The disease-free equilibrium as calculated above is

$$\mathcal{E}^* = (X^*, Y^*) = \left(0^7, \left(\frac{\Delta}{a_7 + \mu}, 0, \frac{a_7 \Delta}{(a_7 + \mu)(a_8 + \mu)}, \frac{a_7 a_8 \Delta}{\mu (a_7 + \mu)(a_8 + \mu)}, \frac{\Delta_V}{\mu_V} \right) \right). \tag{53}$$

Then one finds the following matrices $F = \frac{\partial \mathcal{F}_i(0, Y^*)}{\partial X_j}$ and $V = \frac{\partial \mathcal{V}_i(0, Y^*)}{\partial X_j}$:

$$F = \begin{pmatrix} 0 & \delta_{HH} f_{I_1} \mathtt{A} & \delta_{HH} f_{I_2} \mathtt{A} & \delta_{HH} f_D f_{I_1} \mathtt{A} & \delta_{HH} f_D f_{I_2} \mathtt{A} & \delta_{VH} \mathtt{A} \cdot \frac{\Delta \mu_V}{\mu \Delta_V} & \delta_{PH} f_P \mathtt{A} \\ 0 & \delta_{HH} f_{I_1} \mathtt{B} & \delta_{HH} f_{I_2} \mathtt{B} & \delta_{HH} f_D f_{I_1} \mathtt{B} & \delta_{HH} f_D f_{I_2} \mathtt{B} & \delta_{VH} \mathtt{B} \cdot \frac{\Delta \mu_V}{\mu \Delta_V} & \delta_{PH} f_P \mathtt{B} \\ 0 & 0 & 0 & 0 & 0 & 0 & 0 \\ 0 & 0 & 0 & 0 & 0 & 0 & 0 \\ 0 & 0 & 0 & 0 & 0 & 0 & 0 \\ 0 & a_{18} \delta_{HV} f_{I_1} \frac{\Delta_V \mu}{\mu_V \Delta} & a_{18} \delta_{HV} f_{I_2} \frac{\Delta_V \mu}{\mu_V \Delta} & a_{18} \delta_{HV} f_D f_{I_1} \frac{\Delta_V \mu}{\mu_V \Delta} & a_{18} \delta_{HV} f_D f_{I_2} \frac{\Delta_V \mu}{\mu_V \Delta} & a_{18} \delta_{VV} & 0 \\ 0 & \alpha_P f_{I_1} & \alpha_P f_{I_2} & \alpha_P f_D f_{I_1} & \alpha_P f_D f_{I_2} & 0 & 0 \end{pmatrix}, \tag{54}$$

with

$$\mathtt{A} = a_1 \frac{S^*}{N^*} + a_{10} \frac{V_1^*}{N^*} + a_9 \frac{V_2^*}{N^*} = \frac{a_1 \mu (a_8 + \mu) + a_7 a_{10} \mu + a_7 a_8 a_9}{(a_7 + \mu)(a_8 + \mu)} \tag{55}$$

$$\mathtt{B} = a_5 \frac{S^*}{N^*} + a_{11} \frac{V_1^*}{N^*} + a_{12} \frac{V_2^*}{N^*} = \frac{a_5 \mu (a_8 + \mu) + a_7 a_{11} \mu + a_7 a_8 a_{12}}{(a_7 + \mu)(a_8 + \mu)}, \tag{56}$$

and

$$V = \begin{pmatrix} a_2 + \mu & 0 & 0 & 0 & 0 & 0 & 0 \\ -a_2 & a_3 + a_6 + a_{13} + \mu_{I_1} & 0 & 0 & 0 & 0 & 0 \\ 0 & -a_3 & a_4 + a_{16} + \mu_{I_2} & 0 & 0 & 0 & 0 \\ 0 & -a_{13} & 0 & a_{14} + a_{15} + \mu_{I_1} & 0 & 0 & 0 \\ 0 & 0 & -a_{16} & -a_{14} & a_{17} + \mu_{I_2} & 0 & 0 \\ 0 & 0 & 0 & 0 & 0 & \mu_V & 0 \\ 0 & 0 & 0 & 0 & 0 & 0 & \mu_P \end{pmatrix} \tag{57}$$

The next-generation matrix $K := FV^{-1}$ (the inverse V^{-1} is provided in the Appendix) reads:

$$K = \begin{pmatrix} \delta_{HH}\mathtt{AC} & \delta_{HH}\mathtt{AD} & \delta_{HH}\mathtt{AE} & \delta_{HH}\mathtt{AF} & \delta_{HH}\mathtt{A}\frac{f_D f_{I_2}}{a_{17}+\mu_{I_2}} & \delta_{VH}\mathtt{A}\frac{\Delta}{\mu\Delta_V} & \delta_{PH}\mathtt{A}\frac{f_P}{\mu_P} \\ \delta_{HH}\mathtt{BC} & \delta_{HH}\mathtt{BD} & \delta_{HH}\mathtt{BE} & \delta_{HH}\mathtt{BF} & \delta_{HH}\mathtt{B}\frac{f_D f_{I_2}}{a_{17}+\mu_{I_2}} & \delta_{VH}\mathtt{B}\frac{\Delta}{\mu\Delta_V} & \delta_{PH}\mathtt{B}\frac{f_P}{\mu_P} \\ 0 & 0 & 0 & 0 & 0 & 0 & 0 \\ 0 & 0 & 0 & 0 & 0 & 0 & 0 \\ 0 & 0 & 0 & 0 & 0 & 0 & 0 \\ \delta_{HV}a_{18}\frac{\Delta_V\mu}{\mu_V\Delta}\mathtt{C} & \delta_{HV}a_{18}\frac{\Delta_V\mu}{\mu_V\Delta}\mathtt{D} & \delta_{HV}a_{18}\frac{\Delta_V\mu}{\mu_V\Delta}\mathtt{E} & \delta_{HV}a_{18}\frac{\Delta_V\mu}{\mu_V\Delta}\mathtt{F} & \delta_{HV}a_{18}\frac{\Delta_V\mu}{\mu_V\Delta}\frac{f_D f_{I_2}}{a_{17}+\mu_{I_2}} & \delta_{VV}\frac{a_{18}}{\mu_V} & 0 \\ \alpha_P\mathtt{C} & \alpha_P\mathtt{D} & \alpha_P\mathtt{E} & \alpha_P\mathtt{F} & \alpha_P\frac{f_D f_{I_2}}{a_{17}+\mu_{I_2}} & 0 & 0 \end{pmatrix}, \tag{58}$$

with

$$\mathtt{A} = \frac{a_1\mu\left(a_8+\mu\right)+a_7a_{10}\mu+a_7a_8a_9}{\left(a_7+\mu\right)\left(a_8+\mu\right)} \text{ as before} \tag{59}$$

$$\mathtt{B} = \frac{a_5\mu\left(a_8+\mu\right)+a_7a_{11}\mu+a_7a_8a_{12}}{\left(a_7+\mu\right)\left(a_8+\mu\right)} \text{ as before} \tag{60}$$

$$\begin{aligned}\mathtt{C} =& \frac{f_{I_1}a_2}{(a_2+\mu)\left(a_3+a_6+a_{13}+\mu_{I_1}\right)} + \frac{f_{I_2}a_2a_3}{(a_2+\mu)\left(a_3+a_6+a_{13}+\mu_{I_1}\right)\left(a_4+a_{16}+\mu_{I_2}\right)} \\ &+ \frac{f_D f_{I_1}a_2a_{13}}{(a_2+\mu)\left(a_3+a_6+a_{13}+\mu_{I_1}\right)\left(a_{14}+a_{15}+\mu_{I_1}\right)} \\ &+ \frac{f_D f_{I_2}a_2\left(a_3a_{16}\left(a_{14}+a_{15}+\mu_{I_1}\right)+a_{13}a_{14}\left(a_4+a_{16}+\mu_{I_2}\right)\right)}{(a_2+\mu)\left(a_3+a_6+a_{13}+\mu_{I_1}\right)\left(a_4+a_{16}+\mu_{I_2}\right)\left(a_{14}+a_{15}+\mu_{I_1}\right)\left(a_{17}+\mu_{I_2}\right)}\end{aligned} \tag{61}$$

$$\begin{aligned}\mathtt{D} =& \frac{f_{I_1}}{a_3+a_6+a_{13}+\mu_{I_1}} + \frac{f_{I_2}a_3}{\left(a_3+a_6+a_{13}+\mu_{I_1}\right)\left(a_4+a_{16}+\mu_{I_2}\right)} + \frac{f_D f_{I_1}a_{13}}{\left(a_3+a_6+a_{13}+\mu_{I_1}\right)\left(a_{14}+a_{15}+\mu_{I_1}\right)} \\ &+ \frac{f_D f_{I_2}\left(a_3a_{16}\left(a_{14}+a_{15}+\mu_{I_1}\right)+a_{13}a_{14}\left(a_4+a_{16}+\mu_{I_2}\right)\right)}{\left(a_3+a_6+a_{13}+\mu_{I_1}\right)\left(a_4+a_{16}+\mu_{I_2}\right)\left(a_{14}+a_{15}+\mu_{I_1}\right)\left(a_{17}+\mu_{I_2}\right)}\end{aligned} \tag{62}$$

$$\mathtt{E} = \frac{f_{I_2}}{a_4+a_{16}+\mu_{I_2}} + \frac{f_D f_{I_2}a_{16}}{\left(a_4+a_{16}+\mu_{I_2}\right)\left(a_{17}+\mu_{I_2}\right)} \tag{63}$$

$$\mathtt{F} = \frac{f_D f_{I_1}}{a_{14}+a_{15}+\mu_{I_1}} + \frac{f_D f_{I_2}a_{14}}{\left(a_{14}+a_{15}+\mu_{I_1}\right)\left(a_{17}+\mu_{I_2}\right)} \tag{64}$$

Since $\mathcal{R}_0 = \rho(K)$, the dominating eigenvalue of this matrix is needed. Using the Laplace expansion, the three rows of zero already reduce the corresponding characteristic polynomial (note that here λ denotes the corresponding eigenvalues, not the infectious term from above) to:

$$\mathcal{X}(\lambda) = -\lambda^3\begin{vmatrix} \delta_{HH}\mathtt{AC}-\lambda & \delta_{HH}\mathtt{AD} & \delta_{VH}\mathtt{A}\frac{\Delta}{\mu\Delta_V} & \delta_{PH}\mathtt{A}\frac{f_P}{\mu_P} \\ \delta_{HH}\mathtt{BC} & \delta_{HH}\mathtt{BD}-\lambda & \delta_{VH}\mathtt{B}\frac{\Delta}{\mu\Delta_V} & \delta_{PH}\mathtt{B}\frac{f_P}{\mu_P} \\ \delta_{HV}a_{18}\frac{\Delta_V\mu}{\mu_V\Delta}\mathtt{C} & \delta_{HV}a_{18}\frac{\Delta_V\mu}{\mu_V\Delta}\mathtt{D} & \delta_{VV}\frac{a_{18}}{\mu_V}-\lambda & 0 \\ \alpha_P\mathtt{C} & \alpha_P\mathtt{D} & 0 & -\lambda \end{vmatrix} \tag{65}$$

As the computation of the determinant of a 4×4 matrix remains quite intricate, potentially yielding multiple non-zero eigenvalues, it becomes inconvenient, if not impossible, to identify the one with the largest absolute value in this general form. Progressing further into these universal calculations without specific characterizations seems unpromising. Unsurprisingly, the function $\mathcal{X}(\lambda)$ is highly contingent on the precise structure of the model. The presence of various δ terms throughout the matrix underscores the significance of distinct transmission pathways for $\mathcal{R}_0$. When the model is applied to a specific pathogen, many of these indicator values turn to zero, as not all transition rates are typically considered simultaneously. In most referenced underlying models, various modes of pathogen transmission are not concurrently integrated. Some diseases do not propagate through vector populations, or if there are multiple biologically feasible transmission pathways, they might not all be of equal importance. For instance, a smear infection might be disregarded if direct inter-human transmission dominates the overall dynamics. Therefore, a logical approach involves considering different transmission paths separately, a choice that not only makes sense but also simplifies both the model and the corresponding next-generation matrix significantly.

Only inter-human transmissions. In the most simple case, the disease only spreads among humans in direct interactions ($\delta_{HH} = 1$). This is the case in the basic Kermack–McKendrick model [9] as well as in many other epidemiological models [6–8,16,24]. No vector population is involved ($\delta_{VH} = \delta_{HV} = \delta_{VV} = 0$) and smear infections do not play a role ($\delta_{PH} = \alpha_P = 0$). This leads to the characteristic polynomial:

$$\mathcal{X}(\lambda) = -\lambda^3\begin{vmatrix} \mathtt{AC}-\lambda & \mathtt{AD} & 0 & 0 \\ \mathtt{BC} & \mathtt{BD}-\lambda & 0 & 0 \\ 0 & 0 & -\lambda & 0 \\ 0 & 0 & 0 & -\lambda \end{vmatrix} = -\lambda^5\left[(\mathtt{AC}-\lambda)(\mathtt{BD}-\lambda)-\mathtt{ABCD}\right] = \lambda^6(\mathtt{AC}+\mathtt{BD}-\lambda). \tag{66}$$

The reproduction rate therefore is the only non-zero eigenvalue

$$\mathcal{R}_0{}^{HH} = \mathtt{AC}+\mathtt{BD}. \tag{67}$$

The definitions of A, B, C and D indicate that this remains a complex term, albeit with some convenient properties. For instance, one typically either considers a compartment E without a direct transition from S, with V_1 and V_2 going directly to I_1 ($a_5 = a_{11} = a_{12} = 0$), or omits such a latent compartment altogether ($a_1 = a_9 = a_{10} = 0$), resulting in either $\mathtt{AC} = 0$ or $\mathtt{BD} = 0$. This simplification aids in formulating the reproduction rate. Examining individual parameters and tracing their influence on the reproduction rate allows for plausibility checks.

For instance, an increased death rate (μ same as μ_I) of humans relevantly reduces C and D and, consequently, decreases ${\mathcal{R}_0}^{HH}$. This aligns with the logic that infected individuals have less time to infect others, if they die faster. Similarly, an elevated fraction of infectiousness for different infectious compartments (f_{I_1}, f_{I_2} and f_D) results in higher reproduction rates. Increasing the detection rate or the speed of detection (both increasing a_{13} and a_{16}) reduces the emphasis on f_{I_1} and f_{I_2} in favor of $f_D f_{I_1}$ and $f_D f_{I_2}$. Assuming that detected individuals are less infectious than undetected ($f_D < 1$), this also decreases ${\mathcal{R}_0}^{HH}$. In the opposite case, $f_D > 1$ would increase the reproduction rate. While formal proofs are not provided here, the overall trend is evident when considering the limits of the parameters approaching either zero or infinity.

Only environmental pathogen. When exclusively considering transmissions through an environmental pathogen ($\delta_{PH} = 1$, $\alpha_P > 0$), while discounting direct human interactions and animal hosts as irrelevant factors ($\delta_{HH} = \delta_{VH} = \delta_{HV} = \delta_{VV} = 0$), the characteristic polynomial is as follows:

$$\mathcal{X}(\lambda) = -\lambda^3 \begin{vmatrix} -\lambda & 0 & 0 & \mathtt{A}\frac{f_P}{\mu_P} \\ 0 & -\lambda & 0 & \mathtt{B}\frac{f_P}{\mu_P} \\ 0 & 0 & -\lambda & 0 \\ \alpha_P \mathtt{C} & \alpha_P \mathtt{D} & 0 & -\lambda \end{vmatrix} = \lambda^4 \begin{vmatrix} -\lambda & 0 & \mathtt{A}\frac{f_P}{\mu_P} \\ 0 & -\lambda & \mathtt{B}\frac{f_P}{\mu_P} \\ \alpha_P \mathtt{C} & \alpha_P \mathtt{D} & -\lambda \end{vmatrix} = \lambda^5 \left[\frac{\alpha_P f_P}{\mu_P} (\mathtt{AC} + \mathtt{BD}) - \lambda^2 \right]. \tag{68}$$

Consequently, the reproduction rate is determined by

$${\mathcal{R}_0}^{PH} = \sqrt{\frac{\alpha_P f_P}{\mu_P} (\mathtt{AC} + \mathtt{BD})} = \sqrt{\frac{\alpha_P f_P}{\mu_P} \cdot {\mathcal{R}_0}^{HH}}. \tag{69}$$

The dynamics are analogous to ${\mathcal{R}_0}^{HH}$, but certain pathogen-specific parameters contribute equally to the value of ${\mathcal{R}_0}^{PH}$. An elevated pathogen spread (α_P) and increased infectiousness (f_P) both elevate the reproduction rate, while a higher death rate (μ_P), potentially resulting from shorter pathogen survival times, diminishes it.

Only vector transmissions. If we consider only a vector population as relevant for the spread of a pathogen, and humans neither infect other humans ($\delta_{HH} = 0$) nor animals ($\delta_{HV} = 0$), and no environmental pathogen is considered ($\alpha_P = \delta_{PH} = 0$), transmissions only occur within the vector species ($\delta_{VV} = 1$) and from vectors to humans, not the other way round ($\delta_{VH} = 1$). This scenario is applicable in models for the spread of avian influenza [22,23]. Here, $\mathcal{X}$ simplifies relevantly to

$$\mathcal{X}(\lambda) = -\lambda^3 \begin{vmatrix} -\lambda & 0 & \mathtt{A}\frac{\Delta}{\mu \Delta_V} & 0 \\ 0 & -\lambda & \mathtt{B}\frac{\Delta}{\mu \Delta_V} & 0 \\ 0 & 0 & \frac{a_{18}}{\mu_V} - \lambda & 0 \\ 0 & 0 & 0 & -\lambda \end{vmatrix} = \lambda^6 \cdot \left(\frac{a_{18}}{\mu_V} - \lambda \right). \tag{70}$$

The reproduction rate is found as the only non-zero eigenvalue of K:

$${\mathcal{R}_0}^{VV} = \frac{a_{18}}{\mu_V} \tag{71}$$

As human interactions do not play any role, all human related parameters do not influence the reproduction rate. As described thoroughly by Maia Martcheva [11], caution is necessary in the interpretation of the reproduction rate here. Since infected hosts are also considered in the next-generation matrix approach, this can be interpreted as the number of secondary cases within the vector population. This becomes clearer with a closer look at the parameters involved in ${\mathcal{R}_0}^{VV}$, as only vector-specific parameters are involved. If the death rate is greater than the inter-vector infection rate $\mu_V > a_{18}$, the disease dies out with ${\mathcal{R}_0}^{VV} < 1$, leading to no more human infections. The disease spreads among the vector population if $a_{18} > \mu_V$. However, it is challenging to deduce the implications for the human population, as this depends on more than only the vector dynamics.

Only inter-species transmissions. If one solely considers transmissions through human-vector interactions (where humans and host animals cannot infect each other within their species), this perspective may be particularly relevant for tick-borne encephalitis as modeled by Akram et al. [18] ($\delta_{HH} = \delta_{VV} = \alpha_P = \delta_{PH} = 0$ and $\delta_{HV} = \delta_{VH} = 1$), one finds:

$$\mathcal{X}(\lambda) = -\lambda^3 \begin{vmatrix} -\lambda & 0 & \mathtt{A}\frac{\Delta}{\mu \Delta_V} & 0 \\ 0 & -\lambda & \mathtt{B}\frac{\Delta}{\mu \Delta_V} & 0 \\ a_{18}\frac{\Delta_V \mu}{\mu_V \Delta}\mathtt{C} & a_{18}\frac{\Delta_V \mu}{\mu_V \Delta}\mathtt{D} & -\lambda & 0 \\ 0 & 0 & 0 & -\lambda \end{vmatrix} = \lambda^5 \left[\frac{a_{18}}{\mu_V} (\mathtt{AC} + \mathtt{BD}) - \lambda^2 \right], \tag{72}$$

with reproduction rate:

$${\mathcal{R}_0}^{VH} = \sqrt{\frac{a_{18}}{\mu_V} (\mathtt{AC} + \mathtt{BD})} = \sqrt{{\mathcal{R}_0}^{VV} \cdot {\mathcal{R}_0}^{HH}}. \tag{73}$$

In this scenario, both ${\mathcal{R}_0}^{VV}$ and ${\mathcal{R}_0}^{HH}$ contribute equally, as the dynamics of both the human and vector population play a role in the spread of a pathogen. It is crucial to note that the reproduction rate should not be interpreted as secondary cases within the human population alone but rather as the geometric mean of secondary cases within both populations [11]. This can lead to situations where the disease becomes epidemic in one population while (almost) dying out in the other.

Human and vector transmissions. By simultaneously incorporating several transmission dynamics, calculations become more complex; however, in certain scenarios, meaningful results can still be derived. When considering solely human and vector transmissions and neglecting transmissions via environmental pathogens ($\delta_{PH} = \alpha_P = 0$), the following results emerge (detailed calculations provided in the Appendix):

$$\mathcal{X}(\lambda) = -\lambda^5 \left[\lambda^2 - \left(\delta_{HH}\mathcal{R}_0{}^{HH} + \delta_{VV}\mathcal{R}_0{}^{VV}\right)\lambda + \left(\delta_{VV}\delta_{HH} - \delta_{HV}\delta_{VH}\right)\mathcal{R}_0{}^{VH\,2}\right]. \tag{74}$$

$\mathcal{R}_0$ is therefore a combination of $\mathcal{R}_0{}^{HH}$, $\mathcal{R}_0{}^{VV}$ and $\mathcal{R}_0{}^{VH}$:

$$\mathcal{R}_0 = \frac{\delta_{HH}\mathcal{R}_0{}^{HH} + \delta_{VV}\mathcal{R}_0{}^{VV}}{2} + \sqrt{\left(\frac{\delta_{HH}\mathcal{R}_0{}^{HH} + \delta_{VV}\mathcal{R}_0{}^{VV}}{2}\right)^2 - \left(\delta_{VV}\delta_{HH} - \delta_{HV}\delta_{VH}\right)\mathcal{R}_0{}^{VH\,2}}. \tag{75}$$

These findings align with the previously discussed results.

In a scenario where all human and vector-related transmission routes are simultaneously relevant ($\delta_{HH} = \delta_{VH} = \delta_{HV} = \delta_{VV} = 1$), the following relationship holds:

$$\mathcal{R}_0{}^{V\&H} = \mathcal{R}_0{}^{VV} + \mathcal{R}_0{}^{HH}. \tag{76}$$

However, the interpretation of the reproduction rate becomes challenging as it represents a combination of reproduction rates in both the human and the vector populations. With all transmission pathways active, an infected individual (host or human) produces both infected hosts and infected humans. Therefore, the reproduction number in this case is the sum of both. If either δ_{VH} or δ_{HV} is set to zero, the reproduction rate reduces to $\mathcal{R}_0{}^{HH}$ or $\mathcal{R}_0{}^{VV}$, respectively. This can be interpreted as the number of secondary cases either in the human or the host population, as only one of these populations exhibits full epidemic dynamics.

Human and environmental pathogen transmissions. If one assumes that vector hosts are not relevantly involved ($\delta_{VH} = \delta_{HV} = \delta_{VV} = 0$) but pathogen and direct inter-human transmissions are both occurring ($\delta_{HH} = \delta_{PH} = 1, \alpha_P > 0$), the following relations arise:

$$\begin{aligned}
\mathcal{X}(\lambda) &= -\lambda^3 \begin{vmatrix} \mathrm{AC}-\lambda & \mathrm{AD} & 0 & \mathrm{A}\frac{f_P}{\mu_P} \\ \mathrm{BC} & \mathrm{BD}-\lambda & 0 & \mathrm{B}\frac{f_P}{\mu_P} \\ 0 & 0 & -\lambda & 0 \\ \alpha_P\mathrm{C} & \alpha_P\mathrm{D} & 0 & -\lambda \end{vmatrix} \\
&= \lambda^4 \begin{vmatrix} \mathrm{AC}-\lambda & \mathrm{AD} & \mathrm{A}\frac{f_P}{\mu_P} \\ \mathrm{BC} & \mathrm{BD}-\lambda & \mathrm{B}\frac{f_P}{\mu_P} \\ \alpha_P\mathrm{C} & \alpha_P\mathrm{D} & -\lambda \end{vmatrix} \\
&= -\lambda^5 \left[\lambda^2 - (\mathrm{AC}+\mathrm{BD})\lambda - (\mathrm{AC}+\mathrm{BD})\frac{f_P\alpha_P}{\mu_P}\right] \\
&= -\lambda^5 \left[\lambda^2 - \mathcal{R}_0{}^{HH}\lambda - \mathcal{R}_0{}^{PH\,2}\right],
\end{aligned} \tag{77}$$

with the reproduction rate:

$$\mathcal{R}_0{}^{P\&H} = \frac{\mathcal{R}_0{}^{HH}}{2} + \sqrt{\left(\frac{\mathcal{R}_0{}^{HH}}{2}\right)^2 + \mathcal{R}_0{}^{PH\,2}}. \tag{78}$$

Firstly, $\mathcal{R}_0{}^{P\&H}$ is larger than $\mathcal{R}_0{}^{HH}$ or $\mathcal{R}_0{}^{PH}$. This is logical as having more possible transmission routes should increase $\mathcal{R}_0$. Secondly, both involved reproduction rates contribute positively, thereby maintaining the general dynamics described in the preceding paragraphs.

3.2. Numerical results

To illustrate the applicability of this general model in real-world scenarios, the following simulations provide a descriptive overview of how the dynamics in this model operate.

In simulating a measles outbreak in Pakistan in 2019, the article by Memon et al. [8] served as a reference due to its close alignment with the new general model. This allows for the replication of simulations by directly adopting variables from their work without the need for refitting parameter values. The values used (see Table 2) are incorporated and, if necessary, converted to align with the specifications of this general model. The replication of the article using our model, along with a plot of vaccination rates, can be found in Fig. 2(a).

By setting parameters of the comprehensive model that are not covered in the original work to zero, certain compartments such as I_2 and D_2 are omitted, and vector population or environmental pathogen are excluded from the figures, as they remain zeros. The exceptionally high vaccination rate of $a_7 = 0.58306$ results in an almost fully vaccinated population of Pakistan, approximately $230,000,000$ [31] within a few months, which is unrealistic. However, the primarily focus here is on the new general ODE model's capability to address various diseases, not on estimating or fitting parameters or improving previously published works. Therefore, all parameter values are directly taken from the original paper without further questioning or commenting on the fitted values found by others. The compartment for second dose vaccinated individuals (V2) is neither used in the original paper, nor in this simulation. To illustrate the general possibility to reduce or enlarge our broad model, this compartment is still depicted in the figure.

Using Eq. (67), the reproduction rate can be computed. With this high vaccination rate, the reproduction rate is found to be very small $\mathcal{R}_V \approx 0.126$. A reproduction rate smaller than one aligns with the disease dying out, which occurs rapidly after the population approaches the equilibrium state with a relevant portion being vaccinated. If the same situation is considered without any vaccination ($a_7 = 0$), the reproduction rate increases to $\mathcal{R}_0 \approx 3.935$. As expected for a reproduction rate clearly greater than one, the disease rapidly spreads throughout the entire population, as depicted in Fig. 2(b) (note the different scales).

Table 2
Parameter values and initial conditions used for simulations. Non listed initial conditions mean that they are set to zero.

Parameter	Measles [8]		Fictitious	
(Δ, Δ_V)	$(260479, 0)$	$\frac{\text{individual}}{\text{month}}$	$(0.15, 0.1)$	$\frac{\text{individual}}{\text{time}}$
(μ, μ_I, μ_V)	$(0.00125, 0, 0)$	$\frac{1}{\text{month}}$	$(0.001, 0.001, 0.001)$	$\frac{1}{\text{time}}$
(α_P, μ_P)	$(0, 0)$	$\frac{1}{\text{month}}$	$(1, 0.1)$	$\frac{1}{\text{time}}$
$\left(f_{I_1}, f_{I_2}, f_D, f_{\mu_{I_2}}, f_1(t), f_P\right)$	$(1, 1, 1, 1, 1, 0)$		$(1, 1, 1, 1, 1, 1)$	
$(a_1, a_2, a_3, a_4, a_5)$	$(36.812, 0.92373, 0, 0, 0)$	$\frac{1}{\text{month}}$	$(10, 1, 1, 1, 0)$	$\frac{1}{\text{time}}$
$(a_6, b_6, a_7, a_8, a_{13}, a_{14})$	$(9.3408, 0, 0.58306, 0, 0, 0)$	$\frac{1}{\text{month}}$	$(0, 0, 0.1, 0.5, 0.1, 1)$	$\frac{1}{\text{time}}$
$(a_{15}, a_{16}, a_{17}, a_{18}, a_{19})$	$(0, 0, 0, 0, 0)$	$\frac{1}{\text{month}}$	$(0, 0.1, 1, 1, 0.01)$	$\frac{1}{\text{time}}$
(e_1, e_2)	$(0.97, 0)$		$(0.9, 1)$	
$(\delta_{HH}, \delta_{HV}, \delta_{VV}, \delta_{VH}, \delta_{PH})$	$(1, 0, 0, 0, 0)$		$(1, 1, 1, 1, 1)$	
Initial values				
$(S, E, I_1, I_2, S_V, I_V, P)_0$	$(23 \cdot 10^7$ [31]$, 0, 237, 0, 0, 0, 0)$	individual	$(97, 1, 1, 1, 99, 1, 1)$	individual

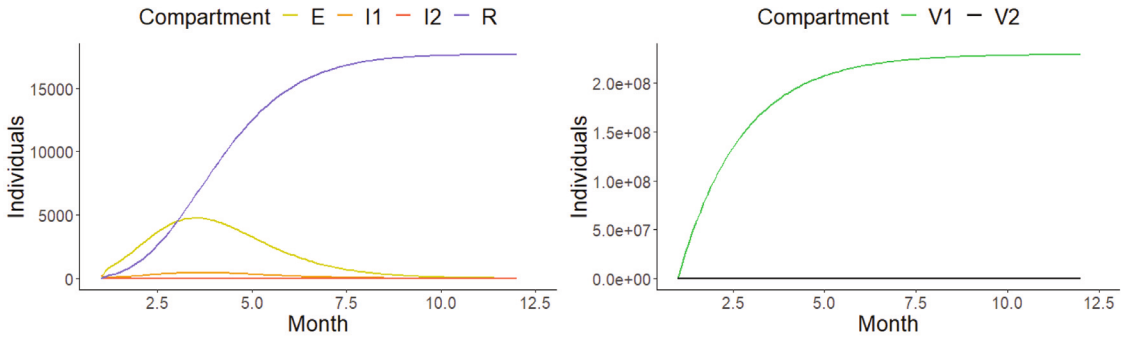

(a) Original simulation with vaccination [8]

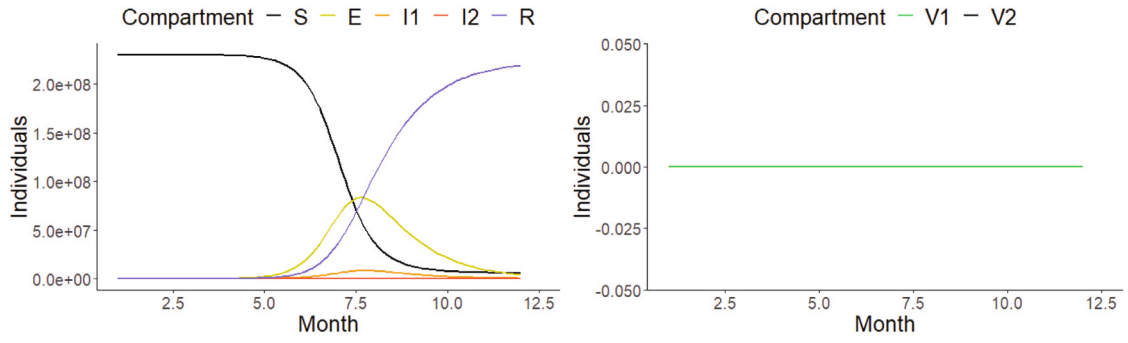

(b) Simulation without vaccination ($a_7 = 0$)

Fig. 2. Simulations of a measles outbreak in Pakistan in 2019 [8] including susceptible (S), exposed (E) first and second stage infected (I1 and I2) and vaccinated (V1) individuals. In 2(a) S is above 200,000,000 and therefore out of scale and left out. To illustrate the general possibility to reduce or enlarge our model, a second dose of vaccination (V2) and a second stage of infection (I2) are depicted in the figures, even though they are not used in the simulations and stay zero. The parameters used for this simulations can be found in Table 2.

To explore some dynamics and properties of the newly developed general model, simulations with fictitious parameters (see Table 2) involving all compartments simultaneously are conducted. A basic set of 100 individuals is chosen, so the results can be interpreted as a percentage. As expected, the disease swiftly progresses through the population and, with some delay, through various compartments from susceptible S to recovered R (see Fig. 3). Similarly, the vector population becomes fully infected, and the pathogen spreads in the environment. Due to the very small detection and vaccination rates (a_{13}, a_{16} and a_7), only a portion of the population gets detected or vaccinated.

This simulation type allows inspection of the influence of particular specifications. For example, an increase in the detection rates to $a_{13} = 1$ and $a_{16} = 1$, leading to a 50% chance of being detected in both stages of infection, along with very strict quarantine measures ($f_D = 0$), results in a slight decrease in infections (Fig. 4(a)). Conversely, increasing the vaccination rate to $a_7 = 1$ leads to dynamics where only 75% end up in the recovered department, while 25% become part of the vaccinated population that managed to escape infection (see Fig. 4(b)).

While it might not be possible to switch transmission routes on and off in a real epidemic, exploring the influence of different transmission routes and checking whether the system's dynamics behave as expected remains an interesting consideration. For instance, considering only inter-human transmissions ($\delta_{HV} = \delta_{VH} = \delta_{VV} = \delta_{PH} = \alpha_P = 0$), significantly slow down infections (see Fig. 4(c)). This is logical as fewer transmissions occur. With Eq. (67), a reproduction rate of $\mathcal{R}_0 \approx 0.118$ is found, leading to the disease dying out once the equilibrium is attained. On the other hand, considering only vector transmissions, as described in the corresponding paragraph above ($\delta_{HH} = \delta_{HV} = \delta_{PH} = \alpha_P = 0$), yields to a reproduction

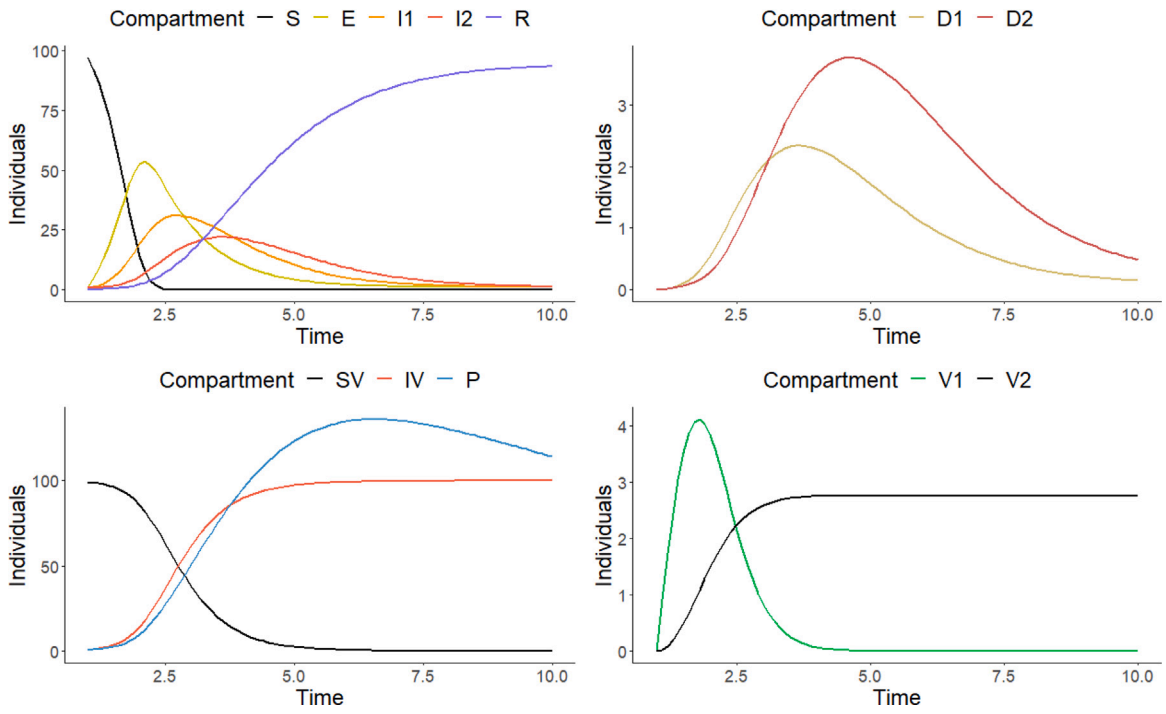

Fig. 3. Fictitious simulations with values from Table 2, depicting susceptible (S), exposed (E), first (I1) and second stage infected (I2), recovered (R), detected (D1 and D2) and vaccinated (V1 and V2) humans and susceptible/infected vectors (SV/IV) as well as a pathogen spread in the environment (P).

rate of $\mathcal{R}_0 = 1000$ (see Eq. (71)). This may seem counterintuitive as infection dynamics within the human population decrease relevantly (Fig. 4(d)). However, as previously described, here the reproduction rate can be interpreted as the reproduction within the vector population, where the disease spreads rapidly, infecting the entire population.

4. Discussion

The here proposed model is versatile and can be applied to a range of different diseases. It integrates the classical SIR model proposed by Kermack and McKendrick [9], which includes compartments for susceptible (S), infected (I_1) and recovered (R) individuals. Additionally, it incorporates an exposed compartment (E) representing a latency phase, as seen in models for measles [8], avian influenza [21] and malaria [19]. A second stage of infection (I_2) is included, following patterns observed in HIV [7] or hepatitis [15,32] models. The model further accounts for two doses of vaccination (V_1 and V_2) with varying levels of immunity, similar to models for measles [16] and COVID [3]. Compartments for detected individuals at each stage of infection (D_1 and D_2) are included to analyze the impact of different pandemic or diagnostic measures. To extend the model's applicability beyond diseases transmitted through direct inter-human contact, a compartment P for environmentally spread pathogens, as seen in the measles model by Alemneh and Belay [14], is incorporated. Additionally, the model accounts for vector populations, as seen in models for diseases like malaria [20] and tick-borne encephalitis [18], with susceptible (S_V) and infected (I_V) vector compartments. The model's flexibility allows for reduction to smaller, more specific models by setting parameters to zero when certain dynamics are not relevant for a particular purpose. For example, setting all transition rates to zero except for a_5 and a_6 results in the classical Kermack and McKendrick model [9]. This reduction to customized sub-models maintains basic properties such as boundedness and non-negativity. For many cases even the formulas to calculate the reproduction rate are already provided, ready to use.

By employing this new model, readily equipped with basic mathematical analysis tools, one can swiftly address the dynamics of an emerging disease. This enables timely guidance for decision-makers, aiding in the consideration of control strategies and the assessment of the general threat posed by an impending disease outbreak. Although a general formula is derived to compute the reproduction rate $\mathcal{R}_0$ as a central measure during an epidemic, caution is advised in interpreting the reproduction rate as it might reflect dynamics in the vector host population or the environmental pathogen instead of human dynamics. The main purpose of this work is limited to pandemic preparedness in the very early stage of a pandemic or epidemic. For detailed investigations equipped with profound data in a later phase, still a specialized model for the specific purpose should be developed that goes beyond the scope of this work.

While many transition rates remain unspecified beyond being non-negative and Lipschitz continuous, they can be defined as needed, enabling the model to cover specific investigations. For example, the introduction of a faster testing method can be analyzed by defining a_{13} and a_{16} as the product of the testing rate and sensitivity divided by the test duration. To incorporate further seasonal dynamics, like seasonal fluctuations in population dynamics for the vector population, the transition rates and other parameters can even be defined as time dependent functions. As long as they are Lipschitz continuous and bounded, all proofs still stay valid or can easily be adjusted. Furthermore, to some extent, it is possible to extract information about compartments that are not explicitly modeled. For instance, if only a known rate of detected individuals can be treated with medication, the infectiousness can be calculated as the weighted mean of untreated and treated detected individuals, consolidated in D_1 and D_2. The model remains open to various specializations beyond those explicitly discussed, increasing compatibility with different research questions.

The model presented here is highly flexible and capable of simulating various diseases, yet it is limited to basic structures. The model's generality can be enhanced by incorporating spatial or social structures to provide differentiated responses, such as those based on age. Additionally, this

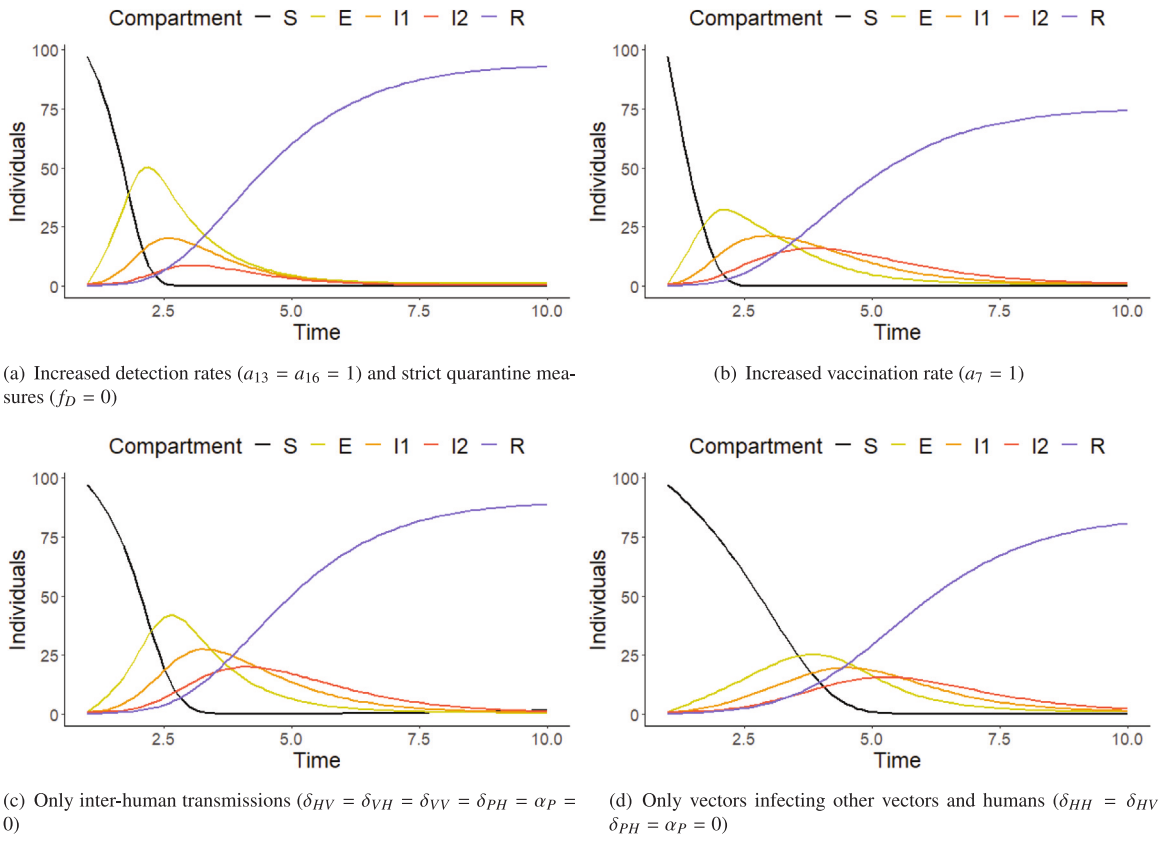

(a) Increased detection rates ($a_{13} = a_{16} = 1$) and strict quarantine measures ($f_D = 0$)

(b) Increased vaccination rate ($a_7 = 1$)

(c) Only inter-human transmissions ($\delta_{HV} = \delta_{VH} = \delta_{VV} = \delta_{PH} = \alpha_P = 0$)

(d) Only vectors infecting other vectors and humans ($\delta_{HH} = \delta_{HV} = \delta_{PH} = \alpha_P = 0$)

Fig. 4. Comparison of fictitious simulations (see Table 2 for parameter values) with some modifications, depicting susceptible (S), exposed (E), first (I1) and second stage infected (I2), recovered (R), detected (D1 and D2) and vaccinated (V1 and V2) individuals.

model currently applies only to deterministic settings, making it suitable for larger populations and case counts. For epidemics in the very early stages with a small number of cases, probabilistic approaches should be applied and would require separate investigation. Probabilistic models could also capture finer dynamics, such as individuals exposed to the virus who do not develop an infection due to a rapid immune response, which are neglected in this deterministic setting.

This model focuses exclusively on human epidemic dynamics, therefore not including exposed vector compartments and considering only one vector population. Consequently, it cannot distinguish between wild and domestic animals. To model more detailed vector dynamics, such as those for avian influenza [22,23], additional compartments would be required to separate susceptible and infected wild and domestic animals. If the development stages of a vector population need to be examined in more detail, the current compartments only differentiating between susceptible and infected vectors, are not sufficient. For instance, a model that explicitly includes different larval stages of a tick population, as in [26], is not feasible with the present model. Furthermore, unlike the influenza model proposed by Kanyiri [6], different strains of a pathogen are not explicitly incorporated. To achieve this, separate parallel compartments for populations infected with each strain would be necessary.

The primary objective of this general model is to enable rapid analysis during the early stages of pathogen spread, guiding control strategies and assessing the overall hazard posed by emerging diseases. To achieve this, the model simplifies human and vector populations into homogeneous groups, without explicitly accounting for individual differences in immune responses or resistances. It focuses on mean values for the entire population, which suffices for analyzing overall dynamics. While increased death rates for recovered individuals due to long-term damage post-infection are not included, these could be incorporated by adding an additional death rate to the recovered compartment. This would require detailed knowledge about long-term excess mortality, which is unlikely to be available at the start of an epidemic. To maintain clarity and simplicity, the model excludes many compartments identified in disease-specific publications. For example, it does not separate intensive care treatments from other treatments, as seen in the COVID model by Fuderer and colleagues [3]. Our model distinguishes only between detected and undetected individuals, preventing further differentiation within the detected population regarding treatment methods or disease severity. Including additional compartments for intensive care or various medications would be necessary for such differentiation.

Despite the simplistic nature of the model, it is designed to cover a wide range of scenarios, allowing for various investigations. This flexibility enables the analysis of potential interventions, such as increasing testing capacities, expediting testing methods, and launching vaccination campaigns. Although specific elements like a separate compartment for quarantine are not explicitly included, the model's consideration of different factors affecting the infectivity of detected individuals allows for in-depth investigations.

CRediT authorship contribution statement

Christoph Sticha: Writing – review & editing, Writing – original draft, Visualization, Validation, Software, Methodology, Investigation, Formal analysis, Conceptualization. **Francesco Picasso:** Writing – review & editing, Validation, Formal analysis. **Christina Kuttler:** Writing – review & editing, Investigation, Formal analysis. **Michael Hoelscher:** Writing – review & editing, Supervision, Investigation, Conceptualization. **Andreas**

Wieser: Writing – review & editing, Supervision, Investigation, Conceptualization. **Noemi Castelletti:** Writing – review & editing, Visualization, Supervision, Project administration, Investigation, Conceptualization.

Declaration of competing interest

The authors declare that they have no known competing financial interests or personal relationships that could have appeared to influence the work reported in this paper.

Data availability

Data is publicly available and cited in the manuscript.

Acknowledgments

F. Picasso acknowledges financial support by the German Federal Ministry of Education and Research (BMBF) (EMUNE/031L0293).

Appendix A. Intermediate results for the next generation matrix

In Section 3.1.4 the reproduction rates are calculated using the next generation matrix approach [11]. The inverse of matrix V reads:

$$V^{-1} = \begin{pmatrix} \frac{1}{a_2+\mu} & 0 & \cdots \\ \frac{a_2}{(a_2+\mu)\left(a_3+a_6+a_{13}+\mu_{I_1}\right)} & \frac{1}{a_3+a_6+a_{13}+\mu_{I_1}} & \\ \frac{a_2 a_3}{(a_2+\mu)\left(a_3+a_6+a_{13}+\mu_{I_1}\right)\left(a_4+a_{16}+\mu_{I_2}\right)} & \frac{a_3}{\left(a_3+a_6+a_{13}+\mu_{I_1}\right)\left(a_4+a_{16}+\mu_{I_2}\right)} & \\ \frac{a_2 a_{13}}{(a_2+\mu)\left(a_3+a_6+a_{13}+\mu_{I_1}\right)\left(a_{14}+a_{15}+\mu_{I_1}\right)} & \frac{a_{13}}{\left(a_3+a_6+a_{13}+\mu_{I_1}\right)\left(a_{14}+a_{15}+\mu_{I_1}\right)} & \\ \frac{a_2\left(a_3 a_{16}\left(a_{14}+a_{15}+\mu_{I_1}\right)+a_{13}a_{14}\left(a_4+a_{16}+\mu_{I_2}\right)\right)}{(a_2+\mu)\left(a_3+a_6+a_{13}+\mu_{I_1}\right)\left(a_4+a_{16}+\mu_{I_2}\right)\left(a_{14}+a_{15}+\mu_{I_1}\right)\left(a_{17}+\mu_{I_2}\right)} & \frac{a_3 a_{16}\left(a_{14}+a_{15}+\mu_{I_1}\right)+a_{13}a_{14}\left(a_4+a_{16}+\mu_{I_2}\right)}{\left(a_3+a_6+a_{13}+\mu_{I_1}\right)\left(a_4+a_{16}+\mu_{I_2}\right)\left(a_{14}+a_{15}+\mu_{I_1}\right)\left(a_{17}+\mu_{I_2}\right)} & \\ 0 & 0 & \\ 0 & 0 & \end{pmatrix} \tag{A.1}$$

$$\begin{pmatrix} 0 & 0 & 0 & 0 & 0 \\ 0 & 0 & 0 & 0 & 0 \\ \frac{1}{a_4+a_{16}+\mu_{I_2}} & 0 & 0 & 0 & 0 \\ 0 & \frac{1}{a_{14}+a_{15}+\mu_{I_1}} & 0 & 0 & 0 \\ \frac{a_{16}}{\left(a_4+a_{16}+\mu_{I_2}\right)\left(a_{17}+\mu_{I_2}\right)} & \frac{a_{14}}{\left(a_{14}+a_{15}+\mu_{I_1}\right)\left(a_{17}+\mu_{I_2}\right)} & \frac{1}{a_{17}+\mu_{I_2}} & 0 & 0 \\ 0 & 0 & 0 & \frac{1}{\mu_V} & 0 \\ 0 & 0 & 0 & 0 & \frac{1}{\mu_P} \end{pmatrix}$$

Appendix B. Intermediate results for the reproduction rate of human and vector transmissions

The characteristic polynomial in paragraph "Human and vector transmissions" of Section 3.1.4 is derived as follows:

$$\begin{aligned} \mathcal{X}(\lambda) &= -\lambda^3 \begin{vmatrix} \delta_{HH}\mathrm{AC}-\lambda & \delta_{HH}\mathrm{AD} & \delta_{VH}\mathrm{A}\frac{\Delta}{\mu\Delta_V} & 0 \\ \delta_{HH}\mathrm{BC} & \delta_{HH}\mathrm{BD}-\lambda & \delta_{VH}\mathrm{B}\frac{\Delta}{\mu\Delta_V} & 0 \\ \delta_{HV}a_{18}\frac{\Delta_V\mu}{\mu_V\Delta}\mathrm{C} & \delta_{HV}a_{18}\frac{\Delta_V\mu}{\mu_V\Delta}\mathrm{D} & \delta_{VV}\frac{a_{18}}{\mu_V}-\lambda & 0 \\ 0 & 0 & 0 & -\lambda \end{vmatrix} \\ &= \lambda^4 \begin{vmatrix} \delta_{HH}\mathrm{AC}-\lambda & \delta_{HH}\mathrm{AD} & \delta_{VH}\mathrm{A}\frac{\Delta}{\mu\Delta_V} \\ \delta_{HH}\mathrm{BC} & \delta_{HH}\mathrm{BD}-\lambda & \delta_{VH}\mathrm{B}\frac{\Delta}{\mu\Delta_V} \\ \delta_{HV}a_{18}\frac{\Delta_V\mu}{\mu_V\Delta}\mathrm{C} & \delta_{HV}a_{18}\frac{\Delta_V\mu}{\mu_V\Delta}\mathrm{D} & \delta_{VV}\frac{a_{18}}{\mu_V}-\lambda \end{vmatrix} \\ &= \lambda^4 \left[\left(\delta_{HH}\mathrm{AC}-\lambda\right)\left(\delta_{HH}\mathrm{BD}-\lambda\right)\left(\delta_{VV}\frac{a_{18}}{\mu_V}-\lambda\right) + 2\delta_{HH}\delta_{HV}\delta_{VH}\mathrm{ABCD}\frac{a_{18}}{\mu_V} \right. \\ &\quad \left. -\delta_{HV}\delta_{VH}\mathrm{AC}\frac{a_{18}}{\mu_V}\left(\delta_{HH}\mathrm{BD}-\lambda\right) - \delta_{HV}\delta_{VH}\mathrm{BD}\frac{a_{18}}{\mu_V}\left(\delta_{HH}\mathrm{AC}-\lambda\right) - \delta_{HH}^2\mathrm{ABCD}\left(\delta_{VV}\frac{a_{18}}{\mu_V}-\lambda\right) \right] \\ &= \lambda^4 \left[\left(\lambda^2 - \delta_{HH}\mathrm{AC}\lambda - \delta_{HH}\mathrm{BD}\lambda\right)\left(\delta_{VV}\frac{a_{18}}{\mu_V}-\lambda\right) + \delta_{HV}\delta_{VH}\mathrm{AC}\frac{a_{18}}{\mu_V}\lambda + \delta_{HV}\delta_{VH}\mathrm{BD}\frac{a_{18}}{\mu_V}\lambda \right] \\ &= \lambda^5 \left[\delta_{VV}\frac{a_{18}}{\mu_V}\lambda - \delta_{VV}\delta_{HH}\mathrm{AC}\frac{a_{18}}{\mu_V} - \delta_{VV}\delta_{HH}\mathrm{BD}\frac{a_{18}}{\mu_V} - \lambda^2 + \delta_{HH}\mathrm{AC}\lambda + \delta_{HH}\mathrm{BD}\lambda \right. \\ &\quad \left. +\delta_{HV}\delta_{VH}\mathrm{AC}\frac{a_{18}}{\mu_V} + \delta_{HV}\delta_{VH}\mathrm{BD}\frac{a_{18}}{\mu_V} \right] \\ &= -\lambda^5 \left[\lambda^2 - \left(\delta_{HH}\left(\mathrm{AC}+\mathrm{BD}\right) + \delta_{VV}\frac{a_{18}}{\mu_V}\right)\lambda + \left(\delta_{VV}\delta_{HH} - \delta_{HV}\delta_{VH}\right)\left(\mathrm{AC}+\mathrm{BD}\right)\frac{a_{18}}{\mu_V} \right] \\ &= -\lambda^5 \left[\lambda^2 - \left(\delta_{HH}{\mathcal{R}_0}^{HH} + \delta_{VV}{\mathcal{R}_0}^{VV}\right)\lambda + \left(\delta_{VV}\delta_{HH} - \delta_{HV}\delta_{VH}\right){\mathcal{R}_0}^{VH^2} \right] \end{aligned} \tag{B.1}$$

References

[1] Barbarossa MV, Fuhrmann J, Meinke JH, Krieg S, Varma HV, Castelletti N, Lippert T. Modeling the spread of COVID-19 in Germany: Early assessment and possible scenarios. PLOS ONE 2020;15(9):e0238559. http://dx.doi.org/10.1371/journal.pone.0238559.

[2] Contento L, Castelletti N, Raimúndez E, Gleut RL, Schälte Y, Stapor P, Hinske LC, Hoelscher M, Wieser A, Radon K, Fuchs C, Hasenauer J. Integrative modelling of reported case numbers and seroprevalence reveals time-dependent test efficiency and infectious contacts. Epidemics 2023;43:100681. http://dx.doi.org/10.1016/j.epidem.2023.100681.

[3] Fuderer S, Kuttler C, Hoelscher M, Hinske LC, Castelletti N. Data suggested hospitalization as critical indicator of the severity of the COVID-19 pandemic, even at its early stages. Math Biosci Eng 2023;20(6):10304–38. http://dx.doi.org/10.3934/mbe.2023452.

[4] van Zandvoort K, Jarvis CI, Pearson CAB, Davies NG, Nightingale ES, Munday JD, Gimma A, Rosello A, Villabona-Arenas J, Funk S, Atkins KE, Diamond C, Meakin SR, Procter SR, Sun FY, Endo A, Tully DC, Rees EM, Deol AK, Foss AM, Klepac P, Edmunds WJ, Prem K, Emery JC, Auzenbergs M, Abbott S, Clifford S, Jombart T, Knight G, Hué S, Leclerc QJ, O'Reilly K, Quilty BJ, Houben RMGJ, Hellewell J, Bosse NI, Gibbs HP, Liu Y, Medley G, Ratnayake R, Russell TW, Kucharski AJ, Jit M, Flasche S, Eggo RM, and FC. Response strategies for COVID-19 epidemics in African settings: a mathematical modelling study. BMC Med 2020;18(1). http://dx.doi.org/10.1186/s12916-020-01789-2.

[5] Zhang X-S, Vynnycky E, Charlett A, Angelis DD, Chen Z, Liu W. Transmission dynamics and control measures of COVID-19 outbreak in China: a modelling study. Sci Rep 2021;11(1). http://dx.doi.org/10.1038/s41598-021-81985-z.

[6] Kanyiri CW, Mark K, Luboobi L. Mathematical analysis of influenza a dynamics in the emergence of drug resistance. Comput Math Methods Med 2018;2018:1–14. http://dx.doi.org/10.1155/2018/2434560.

[7] Arias R, Angeles KD, Maleki S, Ahangar RR. Mathematical modeling of the HIV-AIDS epidemic. OALib 2022;09(02):1–15. http://dx.doi.org/10.4236/oalib.1107972.

[8] Memon Z, Qureshi S, Memon BR. Mathematical analysis for a new nonlinear measles epidemiological system using real incidence data from Pakistan. Eur Phys J Plus 2020;135(4). http://dx.doi.org/10.1140/epjp/s13360-020-00392-x.

[9] Kermack WO, McKendrick AG. A contribution to the mathematical theory of epidemics. Proc R Soc Lond Ser A Math Phys Char 1927;115(772):700–21. http://dx.doi.org/10.1098/rspa.1927.0118.

[10] Müller J, Kuttler C. Methods and models in mathematical biology. Springer Berlin Heidelberg; 2015, http://dx.doi.org/10.1007/978-3-642-27251-6.

[11] Martcheva M. An introduction to mathematical epidemiology. Springer US; 2015, http://dx.doi.org/10.1007/978-1-4899-7612-3.

[12] Schlickeiser R, Kröger M. Analytical modeling of the temporal evolution of epidemics outbreaks accounting for vaccinations. Physics 2021;3(2):386–426. http://dx.doi.org/10.3390/physics3020028.

[13] rnstad ONB, Shea K, Krzywinski M, Altman N. The SEIRS model for infectious disease dynamics. Nat Meth 2020;17(6):557–8. http://dx.doi.org/10.1038/s41592-020-0856-2.

[14] Alemneh HT, Belay AM. Modelling, analysis, and simulation of measles disease transmission dynamics. Discrete Dyn Nat Soc 2023;2023:1–20. http://dx.doi.org/10.1155/2023/9353540.

[15] Mwaijande SE, Mpogolo GE. Modeling the transmission dynamics of hepatitis A with combined vaccination and sanitation mitigation. Comput Math Methods Med 2023;2023:1–19. http://dx.doi.org/10.1155/2023/1203049.

[16] Aldila D, Asrianti D. A deterministic model of measles with imperfect vaccination and quarantine intervention. J Phys Conf Ser 2019;1218(1):012044. http://dx.doi.org/10.1088/1742-6596/1218/1/012044.

[17] Verguet S, Johri M, Morris SK, Gauvreau CL, Jha P, Jit M. Controlling measles using supplemental immunization activities: A mathematical model to inform optimal policy. Vaccine 2015;33(10):1291–6. http://dx.doi.org/10.1016/j.vaccine.2014.11.050.

[18] Akram S, Arooj A, Yasmin N, Ghaffar A, Baleanu D, Nisar KS, Khan I. Standard routine techniques of modeling of tick-borne encephalitis. Open Phys 2020;18(1):820–8. http://dx.doi.org/10.1515/phys-2020-0113.

[19] Kim S, Byun JH, Park A, Jung IH. A mathematical model for assessing the effectiveness of controlling relapse in plasmodium vivax malaria endemic in the Republic of Korea. PLOS ONE 2020;15(1):e0227919. http://dx.doi.org/10.1371/journal.pone.0227919.

[20] Collins O, Duffy K. A mathematical model for the dynamics and control of malaria in Nigeria. Infect Dis Model 2022;7(4):728–41. http://dx.doi.org/10.1016/j.idm.2022.10.005.

[21] Modnak C. Mathematical modelling of an avian influenza: Optimal control study for intervention strategies. Appl Math Inf Sci 2017;11(4):1049–57. http://dx.doi.org/10.18576/amis/110411.

[22] Kimbir AR, Aboiyar T, Okolo PN. A model analysis for the transmission dynamics of avian influenza. Math Theory Model 2014;4:15–28, URL https://api.semanticscholar.org/CorpusID:118226218.

[23] Li Y, Qin P, Zhang J. Dynamics analysis of avian influenza A(H7N9) epidemic model. Discrete Dyn Nat Soc 2018;2018:1–12. http://dx.doi.org/10.1155/2018/7485310.

[24] Bozkurt F, Peker F. Mathematical modelling of HIV epidemic and stability analysis. Adv Difference Equ 2014;2014(1). http://dx.doi.org/10.1186/1687-1847-2014-95.

[25] Berge T, Lubuma J-S, Moremedi G, Morris N, Kondera-Shava R. A simple mathematical model for Ebola in Africa. J Biol Dyn 2016;11(1):42–74. http://dx.doi.org/10.1080/17513758.2016.1229817.

[26] Nah K, Magpantay FMG, Bede-Fazekas Á, Röst G, Trájer AJ, Wu X, Zhang X, Wu J. Assessing systemic and non-systemic transmission risk of tick-borne encephalitis virus in Hungary. PLOS ONE 2019;14(6):e0217206. http://dx.doi.org/10.1371/journal.pone.0217206.

[27] Markus MB. Malaria: Origin of the term "hypnozoite". J History Biol 2010;44(4):781–6. http://dx.doi.org/10.1007/s10739-010-9239-3.

[28] Wang K, Fan H, Zhu Y. Dynamics and application of a generalized SIQR epidemic model with vaccination and treatment. Appl Math Model 2023;120:382–99. http://dx.doi.org/10.1016/j.apm.2023.03.036.

[29] Thieme HR. Mathematics in population biology. Princeton University Press; 2003, http://dx.doi.org/10.1515/9780691187655.

[30] Diekmann O, Heesterbeek J, Metz J. On the definition and the computation of the basic reproduction ratio R 0 in models for infectious diseases in heterogeneous populations. J Math Biol 1990;28(4). http://dx.doi.org/10.1007/bf00178324.

[31] Statista. Pakistan: Gesamtbevölkerung von 1950 bis 2022 und Prognosen bis 2050 (in Millionen Einwohner) [Graph]. 2022, URL https://de.statista.com/statistik/daten/studie/159732/umfrage/gesamtbevoelkerung-von-pakistan/.

[32] Prakasha DG, Veeresha P, Baskonus HM. Analysis of the dynamics of hepatitis E virus using the Atangana-Baleanu fractional derivative. Eur Phys J Plus 2019;134(5). http://dx.doi.org/10.1140/epjp/i2019-12590-5.